Eur Radiol (2012) 22:83–92
DOI 10.1007/s00330-011-2211-6

CHEST

Acute exacerbation of idiopathic pulmonary fibrosis: high-resolution CT scores predict mortality

Kiminori Fujimoto · Hiroyuki Taniguchi · Takeshi Johkoh · Yasuhiro Kondoh · Kazuya Ichikado · Hiromitsu Sumikawa · Takashi Ogura · Kensuke Kataoka · Takahiro Endo · Atsushi Kawaguchi · Nestor L. Müller

Received: 2 March 2011 / Revised: 24 May 2011 / Accepted: 20 June 2011 / Published online: 7 August 2011

Abstract
Objectives To determine high-resolution computed tomography (HRCT) findings helpful in predicting mortality in patients with acute exacerbation of idiopathic pulmonary fibrosis (AEx-IPF).
Methods Sixty patients with diagnosis of AEx-IPF were reviewed retrospectively. Two groups (two observers each) independently evaluated pattern, distribution, and extent of HRCT findings at presentation and calculated an HRCT score at AEx based on normal attenuation areas and extent of abnormalities, such as areas of ground-glass attenuation and/or consolidation with or without traction bronchiectasis or bronchiolectasis and areas of honeycombing. The correlation between the clinical data including the HRCT score and mortality (cause-specific survival) was evaluated using the univariate and multivariate Cox-regression analyses.
Results Serum KL-6 level, $PaCO_2$, and the HRCT score were statistically significant predictors on univariate analysis. Multivariate analysis revealed that the HRCT score was an independently significant predictor of outcome (hazard ratio, 1.13; 95% confidence interval, 1.06–1.19, $P=0.0002$). The area under receiver operating characteristics curve for the HRCT score was statistically significant in the classification of survivors or nonsurvivors (0.944; $P<0.0001$). Survival in patients with HRCT score ≥245 was worse than those with lower score (log-rank test, $P<0.0001$).
Conclusion The HRCT score at AEx is independently related to prognosis in patients with AEx-IPF.
Key Points
• *High-Resolution Computed Tomography (HRCT) helps clinicians to assess patients with interstitial fibrosis.*

K. Fujimoto (✉)
Department of Radiology,
Kurume University School of Medicine, and Center for Diagnostic Imaging, Kurume University Hospital,
67 Asahi-machi,
Kurume, Fukuoka 830-0011, Japan
e-mail: kimichan@med.kurume-u.ac.jp

H. Taniguchi · Y. Kondoh · K. Kataoka
Department of Respiratory Medicine and Allergy,
Tosei General Hospital,
Seto, Aichi, Japan

T. Johkoh
Department of Radiology, Kinki Central Hospital of Mutual Aid Association of Public School Teachers,
Itami, Japan

K. Ichikado
Division of Respiratory Medicine, Saiseikai Kumamoto Hospital,
Kumamoto, Japan

H. Sumikawa
Department of Radiology,
Osaka University Graduate School of Medicine,
Suita, Osaka, Japan

T. Ogura · T. Endo
Department of Respiratory Medicine,
Kanagawa Cardiovascular and Respiratory Center,
Yokohama, Kanagawa, Japan

A. Kawaguchi
Biostatistics Center, Kurume University School of Medicine,
Kurume, Japan

N. L. Müller
Department of Radiology, University of British Columbia and Vancouver General Hospital,
Vancouver, B.C., Canada

- *The main abnormalities of acute exacerbation are ground-glass opacification and consolidation.*
- *Extent of abnormalities on HRCT correlates with poor prognosis.*

Keywords Idiopathic pulmonary fibrosis · Disease exacerbation · Diffuse alveolar damage · High-resolution computed tomography · Mortality

Introduction

Idiopathic pulmonary fibrosis (IPF), pathologically usual interstitial pneumonia (UIP), is the most common idiopathic interstitial pneumonia (IIP) of unknown aetiology [1]. The clinical course of IPF is usually chronic, but some patients may experience episodes of acute respiratory worsening [2–10]. Although these episodes may occur secondary to pneumonia, pulmonary embolism, pneumothorax or cardiac failure, the term "acute exacerbation of IPF (AEx-IPF)" has been used when a cause cannot be identified for the acute respiratory worsening [3–10]. AEx-IPF is characterized histologically by the presence of diffuse alveolar damage (DAD) or, less commonly, organizing pneumonia (OP) superimposed on findings of underlying UIP [9, 11, 12]. The prognosis of AEx-IPF is poor, usually leading to death within a few weeks or months [3–10]. A number of studies have reported on the clinical significance of AEx-IPF [9]; however, there have been a few studies in a limited number of patients assessing the relationship between AEx and baseline known prognostic factors of IPF [13].

High-resolution computed tomography (HRCT) is a useful investigation in the diagnosis and management of AEx-IPF. The characteristic findings consist of new-onset ground-glass opacities and/or consolidation on a background of fibrosis (intralobular reticular opacities and traction bronchiectasis or bronchiolectasis) and honeycombing [4, 9, 12, 14]. One study has suggested that peripheral versus combined multifocal or diffuse distribution on HRCT were predictive of survival in patients with AEx-IPF [14]. However, another study was unable to confirm these findings [12].

In the setting of acute respiratory distress syndrome (ARDS) and acute interstitial pneumonia, both of which are manifested histopathologically DAD, Ichikado et al. [15–18] highlighted the value of parenchymal opacification associated with traction bronchiectasis or bronchiolectasis and areas of honeycombing on HRCT and demonstrated that the overall HRCT score was an important prognostic factor.

The aim of this study was to determine whether an overall HRCT score could be helpful in predicting patient outcome in patients with AEx-IPF.

Patients and methods

Patients

Our institutional review boards, based on the ethical guidelines of the Declaration of Helsinki (2008 version) [19], approved this retrospective study and waived the informed consent requirement.

We reviewed the medical records of all patients who were diagnosed as having AEx-IPF in our three institutions between 1998 and 2007. Patients, (*a*) who fulfilled the American Thoracic Society/European Respiratory Society consensus criteria of IPF [1]; (*b*) who met the criteria of AEx-IPF; and (*c*) who underwent HRCT of the chest at the onset of AEx, were included in the study. AEx-IPF was defined using the revised criteria for AEx-IPF [6, 10], which states that all of the following three conditions must be satisfied during the course of IPF within 1 month: (1) increased dyspnoea, (2) new ground-glass opacities or consolidation appear on HRCT, (3) greater than 10 mmHg decrease in oxygen partial pressure in resting arterial blood (PaO_2) from previous measurements. Obvious causes of these changes, such as infection, pneumothorax, cancer, pulmonary embolism or congestive heart failure, need to be excluded.

Sixty patients met the inclusion criteria: 49 men and 11 women, median age 71 years (range, 37 to 87 years). At the onset of AEx-IPF, there was no evidence of heart failure on both clinical and echocardiographic findings in any of the patients. Cultures of sputum, blood, and urine examined for mycobacteria, fungi, and bacteria were negative in all patients. Bronchoalveolar lavage fluid (BALF) examination at the onset of AEx was successfully performed in 36 patients and all cultures of BALF in 36 patients were negative for infection. Three patients underwent surgical biopsy at the onset of AEx and 2 underwent autopsy. There was no histologic evidence of infection and the pathologic diagnosis of organizing phase DAD was made in all these 5 cases.

All patients received high-dose intravenous corticosteroids (methylprednisolone, 1–2 g/d) for 3 days after the possibility of infection was ruled out by cultures of sputum and serum titers against *Mycoplasma*, *Chlamydia*, *Legionella*, and various viruses. Corticosteroid therapy was followed by a tapered dosage and was combined with intravenous or oral administration of immunosuppressants, such as cyclophosphamide and cyclosporine, in all patients.

Cause-specific survival analysis, survival status, and follow-up periods were assessed by review of the medical records. The median interval between initial diagnosis of IPF and onset of AEx was 17 months (range, 1–120 months). The median follow-up period between the onset of AEx and final

observation day (December 31, 2009) of survivors was 370 days (range, 39–1230 days).

Forty-eight patients died of respiratory failure following AEx despite treatment and the remaining 12 patients responded to medical treatment (the mortality was 80%). In the latter group, 2 of 12 patients died of infectious disease after recovery of acute respiratory failure (died at 228 and 380 days, respectively after onset of AEx), one patient was missing after discharge, and the remaining 9 patients were still alive at the final observation day.

Examination and assessment of HRCT

The HRCT examinations in AEx were obtained at the day of hospitalization and within 4 days (median, 2 days; range, 0–4 days) after onset of symptoms. HRCT data acquisitions were obtained at end inspiration and in the supine position using a variety of CT machines. The protocols consisted of 1- or 2-mm collimation sections reconstructed with a high-spatial-frequency algorithm at 1- or 2-cm intervals. The images were photographed at window settings appropriate for viewing the lung parenchyma (window level −600 to −700 Hounsfield units [HU]; window width 1,200–1,500 HU) and the mediastinum (window level 400–500 HU; window width 20–40 HU).

The images were reviewed in random order by two independent groups of two radiologists who were chest radiologists with 23, 21, 18 and 10 years of experience, respectively. They were informed about the diagnosis of IPF but were unaware of any other clinical findings or patient outcome. In each group, radiologists independently evaluated the presence, extent, and distribution of CT findings, such as ground-glass attenuation (GGA), consolidation, traction bronchiectasis or bronchiolectasis, and honeycombing, as defined by the Fleischner Society [20] and the findings were agreed upon by consensus between the two radiologists for each group. This methodology is based on the method of Sumikawa et al. [21].

The pulmonary opacification, i.e., GGA and consolidation, was classified into peripheral, multifocal, and diffuse patterns according to the CT patterns classification described by Akira et al. [14].

Calculation of HRCT score

The HRCT findings were graded on a one to six scale based on the classification by Ichikado et al. [17, 18] as follows: areas with (*1*) normal attenuation (spared area); (*2*) GGA without traction bronchiectasis or bronchiolectasis; (*3*) consolidation without traction bronchiectasis or bronchiolectasis; (*4*) GGA with traction bronchiectasis or bronchiolectasis; (*5*) consolidation with traction bronchiectasis or bronchiolectasis; and (*6*) honeycombing.

The observers evaluated the extent of all abnormalities to determine the percentage of lung parenchyma occupied by the disease. The lungs were divided into six zones (upper, middle and lower on both sides); each zone was evaluated separately. The upper lung zone was defined as the area of the lung above the level of the tracheal carina, the lower lung zone was defined as the area of the lung below the level of the inferior pulmonary vein, and the middle lung zone was defined as the area of the lung between the upper and lower zones. When abnormal findings were present, the extent of lung involvement was evaluated visually and independently for each of the six lung zones. The score was based on the percentage of the lung parenchyma that showed evidence of the abnormality and was estimated to the nearest 5% of parenchymal involvement. The overall percentage of lung involvement was calculated by averaging the six lung zones for each HRCT finding.

Each abnormality score was calculated multiplying the extent of involvement by each grading score and for each index we drew up an average score of the six lung zones for each patient. The overall HRCT score was obtained by adding the averages of each index as followed formula:

$$\begin{aligned}\text{Overall HRCT score (\%)} = {} & \text{average score of normal attenuation} \times 1 \\ & + \text{average score of GGAwithout traction bronchiectasis or bronchiolectasis} \times 2 \\ & + \text{average score of consolidation without traction bronchiectasis or bronchiolectasis} \times 3 \\ & + \text{average score of GGA with traction bronchiectasis or bronchiolectasis} \times 4 \\ & + \text{average score of consolidation with tractionbronchiectasis or bronchiolectasis} \times 5 \\ & + \text{average score of honeycombing} \times 6.\end{aligned}$$

Table 1 Extent average score of each HRCT finding, interobserver agreement and correlation

HRCT findings[a]	Average scores[b]	Interobserver agreement[d]		Interobserver correlation[e]	
		K value	*P* value	Spearman *r*	*P* value
(1) Spared area	18.3 (8.8–25.0)	0.73	0.0325	0.94	<0.001
(2) GGA without TBE	7.5 (0.4–15.0)	0.67	0.0074	0.85	<0.001
(3) Consolidation without TBE	0 (0–0)[c]	0.70	0.0153	0.71	<0.001
(4) GGA with TBE	36.7 (26.7–54.6)	1.00	<0.001	0.93	<0.0001
(5) Consolidation with TBE	10.0 (3.3–16.7)	0.63	0.0218	0.89	<0.001
(6) Honeycombing	5.0 (1.7–13.3)	0.89	<0.001	0.97	<0.001

[a] HRCT findings: *GGA* areas of ground-glass attenuation; *TBE* traction bronchiectasis or bronchiolectasis

[b] Average scores for overall (mean of the data from two observer groups) are expressed median percentage of lung parenchyma and the 25th to 75th percentile of the interquartile ranges in the parentheses

[c] There were only five cases with positive findings. The mean was 0.18 (range, 1.7–3.3)

[d] Interobserver agreements between two observers are analysed by kappa statistics (*k* value)

[e] Interobserver correlations between two observers are analysed by Spearman's rank correlation test (*r* value)

Statistical analyses

The interobserver variation of the presence/absence of CT findings or the overall impression of the findings was analysed using the *kappa* statistic [22] on the diagnosis made prior to agreement by consensus. Interobserver agreement was classified as follows: poor (k=0–0.20), fair (k=0.21–0.40), moderate (k=0.41–0.60), substantial (k=0.61–0.80) and almost perfect (k=0.81–1.00). The interobserver variation of the extent of the CT findings was evaluated using Spearman's rank correlation coefficient [21]. The overall HRCT scores of the two independent observers' measurements were compared with the Bland-Altman method [23]. After calculating the k values and the Spearman r values for interobserver agreement on the basis of the independent readings, the description of the CT appearance was based on the average of the observations made by the two observer groups when the good agreements between two observer groups were proved.

Continuous variables are expressed in medians and the 25th–75th percentiles of the interquartile range (IQR). The differences of clinical, laboratory, and HRCT data (CT patterns and HRCT scores) between survivors and non-survivors were analysed by using the Mann–Whitney U test or Fisher's test.

Univariate and multivariate analyses using the Cox proportional hazards regression models were used to identify independent patient characteristics, laboratory data and CT predictors of outcome. All variables identified as significant or with P<0.20 were included in the multivariate model. Because the overall HRCT score was calculated based on 6 categories of CT findings, we reanalysed the Cox proportional hazard test to determine which categories related to the prognosis. The diagnostic performance of the HRCT score for predicting patient outcome was assessed with areas under the receiver operating characteristics (ROC) curves. Sensitivity, specificity, positive and negative predictive values (PPV and NPV), positive and negative likelihood ratios (LR) for the classification of survivors and nonsurvivors were calculated with standard formulas according to the optimal cut off value, which was decided on the highest Youden-index

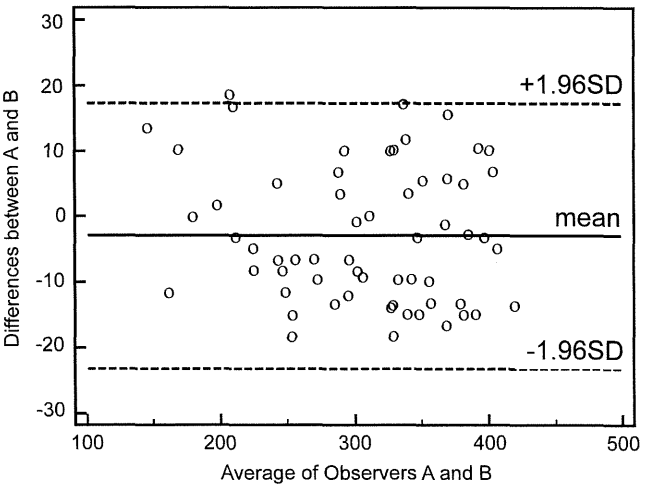

Fig. 1 Bland-Altman plot depict measurement of HRCT score at acute exacerbation of IPF demonstrating good interobserver agreement and lack of proportional bias or fixed bias. The average of the measurements made by the two observers is plotted against the differences between the measurements made by the two observers. The *solid line* represents the mean value of all differences between the two observers, and the *dotted lines* represent the 95% limits of agreement. *SD* = standard deviation

Table 2 Clinical, laboratory and HRCT data in overall, survivors and nonsurvivors at acute exacerbation

Variables[a]	Overall (n=60)	Survivors (n=12)	Nonsurvivors (n=48)	P value
Age, yr	71 (63–75)	74 (71–76)	68 (62–75)	0.071
Gender (Male/Female)	49/11	8/4	41/7	0.140*
Positive smoking history	48	10	38	0.552*
Pack yr	35 (4–49)	37 (30–53)	35 (5–49)	0.636
P/F (mmHg)	214 (106–250)	225 (168–252)	204 (104–250)	0.360
$PaCO_2$ (mmHg)	36.2 (32.5–40.5)	33.6 (31.4–37.5)	36.2 (32.8–41.0)	0.177
LDH (U/L)	404 (308–531)	372 (298–499)	411 (310–534)	0.411
CRP (mg/dL)	7.2 (3.5–12.3)	8.8 (4.5–13.3)	6.8 (3.4–12.3)	0.567
KL-6 (U/mL)	1520 (1102–2072)	1480 (1072–1976)	1520 (1150–2149)	0.657
SP-D (ng/mL)	291 (164–464)	293 (153–480)	291 (166–463)	0.868
CT patterns (p/m/d)[b]	5/11/44	1/5/6	4/6/38	0.062*
HRCT score (%)	320 (245–358)	213 (175–242)	336 (292–371)	<0.0001

[a] Valuables: *P/F* oxygenaton index, PaO_2/fraction of inspired oxygen (FiO_2) mmHg; *LDH* lactate dehydrogenase; *CRP* C-reactive protein; *KL-6* sialylated carbohydrate antigen KL-6; *SP-D* surfactant protein-D

Referential value = LDH, 119–229 U/L; CRP, <0.04 mg/dL; KL-6, <500 U/mL; SP-D, <110 ng/mL

[b] CT patterns: *p* peripheral; *m* multifocal; *d* diffuse

Data were expressed medians and the 25th–75th percentiles of interquartile range

P values: the differences between survivors and nonsurvivors are analyzed by using Mann–Whitney *U* test or Fisher's test*

(i.e., sensitivity + specificity − 1) [24]. Patient survival according to appropriate cut-off value of the HRCT score was determined using the log-rank test and displayed using Kaplan-Meier curves.

For all statistical analyses, a P value of less than 0.05 was considered to indicate a statistically significant difference.

Results

Interobserver agreement

Interobserver agreements in evaluation of presence of CT abnormalities were substantial to almost perfect (*kappa*,

Table 3 Univariate analysis with Cox proportional hazards regression models

Variables[a]	Per unit for HR[c]	HR	95%CI[d]	P value
Age, yr	1-year	0.99	0.96–1.01	0.2774
Gender (Male/Female)	Male	1.20	0.54–2.69	0.6524
Positive Smoking history	positive	0.75	0.38–1.51	0.4205
Pack yr	1-pack yr	0.95	0.86–1.06	0.3642
P/F	10 mmHg	0.98	0.95–1.02	0.3346
$PaCO_2$	5 torr	1.04	1.00–1.08	0.0358
LDH	10 U/L	1.01	0.99–1.02	0.4037
CRP	1 mg/dL	1.01	0.97–1.05	0.8214
KL-6	500 U/mL	1.14	1.00–1.29	0.0446
SP-D	10 ng/mL	1.00	0.99–1.01	0.5326
CT patterns (p/m/d)[b]	m	0.87	0.10–7.62	0.9025
	d	1.34	0.38–4.75	0.6503
HRCT score	10%	1.12	1.06–1.18	<0.0001

[a] Variables: *P/F* oxygenaton index, PaO_2/fraction of inspired oxygen (FiO_2) mmHg;

LDH lactate dehydrogenase; *CRP* C-reactive protein; *KL-6* sialylated carbohydrate antigen KL-6; *SP-D* surfactant protein-D

[b] CT pattern: *p* peripheral; *m* multifocal; *d* diffuse; Peripheral distribution showed no significant difference prognosis compared with multifocal or diffuse distribution of parenchymal opacification

[c] *HR* hazard ratio; HR is calculated with each per unit-increase

[d] *CI* confidence interval

Table 4 Multivariable analysis with Cox proportional hazards regression models

Variables	Per unit for HR[a]	HR	95%CI[b]	*P* value
(1) $PaCO_2$	1 mmHg	1.17	0.92–1.38	0.2531
(2) KL-6	500 U/mL	1.04	0.91–1.18	0.5859
(3) HRCT score	10%	1.13	1.06–1.19	0.0002

[a] *HR* Hazard ratios; HR is calculated with each per unit-increase

[b] *CI* confidence interval

0.63–1.00) (Table 1) and that in assessment of CT pattern was substantial (*kappa*, 0.75). Assessments of extent of CT abnormalities and HRCT scores showed significantly correlation between the two independent groups of observers (Spearman r=0.71–0.97, all P<0.0001) (Table 1). Bland-Altman plots with 95% limits of agreement for the HRCT score is shown in Fig. 1. There was no proportional bias or fixed bias.

Comparisons of clinical, laboratory, and HRCT data between survivors and nonsurvivors

Age, gender, smoking history, arterial blood gas analyses (oxygenation index [P/F] and $PaCO_2$), and serum levels of lactate dehydrogenase (LDH) and C-reactive protein (CRP), and serum markers of interstitial pneumonias [sialylated carbohydrate antigen KL-6 (KL-6) and surfactant protein-D (SP-D)] at the onset of AEx-IPF are summarised in Table 2. The median levels of LDH (384 U/L), CRP (7.2 mg/dL), KL-6 (1,520 U/mL), and SP-D (291 ng/mL) were elevated. The median of P/F (214 mmHg) showed the level of "acute lung injury" according to the American-European Consensus criteria on ARDS [25].

With clinical and laboratory data there was no statistically significant difference between survivors and nonsurvivors (Table 2). The patterns of predominant distribution on CT included peripheral pattern in five patients, multifocal pattern in 11, and diffuse pattern in 44. There was no significant difference between survivors and nonsurvivors among these various patterns (P=0.062, Fisher's test) (Table 2).

The range of overall HRCT score showed 153–411 (median, 320 [IQR, 245–358]). There was a statistically significant difference in the HRCT scores between survivors (median, 213 [IQR, 175–242]) and nonsurvivors (median, 336 [IQR, 292–371]) (Mann–Whitney, P<0.0001).

Univariate and multivariable analyses for survival

Univariate analysis revealed that $PaCO_2$, serum KL-6 values, and the HRCT scores at the onset of AEx were significantly related to prognosis (Table 3). Multivariable analysis revealed that the HRCT score was an independent prognostic factor (hazard ratio [HR] per 10%-increase, 1.13; 95% confidence interval [CI], 1.06–1.19; P=0.0002) (Table 4). In 6 categories for calculating HRCT score, the Cox proportional hazard test revealed that two categories, that were area of GGA with traction bronchiectasis or bronchiolectasis (HR, 1.89; 95%CI, 1.33–2.68; P=0.0004) and area of honeycombing (HR, 1.61; 95%CI, 1.05–2.48; P=0.0280), were important factors for the cause-specific survival (Table 5) (Figs. 2 and 3).

ROC analyses and diagnostic performances for predicting survivors according to HRCT score

The area under the ROC curve of HRCT score were statistically significant in the classification of survivors or nonsurvivors (0.944; 95%CI, 0.879–1.00; P<0.0001). Optimal cut-off value of HRCT score was 245 based on the Youden index, and respective diagnostic performances for predicting the cause-specific survivals are as follows: sensitivity, 0.94 (95%CI, 0.83–0.99); specificity, 0.83 (0.52–0.98); PPV, 0.96 (0.85–0.99); NPV, 0.77 (0.46–0.95); positive LR, 5.63 (2.23–17.16); and negative LR, 0.07 (0.04–0.19), respectively. Patients with a score (≥245) had a significantly worse prognosis than did those with lower score (<245) (log-lank test, P<0.0001) (Fig. 4).

Discussion

In the present study, we demonstrated that the HRCT scoring system showed good interobserver agreement and correlated with mortality in the patients with AEx-IPF. Among 6 categories of CT findings that were used to calculate the HRCT score, areas of GGA with traction bronchiectasis or bronchiolectasis and areas of honeycombing were significantly related to prognosis.

Several studies suggested that survival of patients with AEx-IPF may be related to the degree of CT involvement, such as parenchymal opacification superimposed on under-

Table 5 Multivariable analysis for HRCT score categories

Variables (10%-increase)	HR[a]	95%CI[b]	*P* value
(1) Spared area	1.05	0.68–1.61	0.8710
(2) GGA without TBE	1.33	0.73–2.39	0.3506
(3) Consolidation without TBE	0.74	0.35–1.57	0.4370
(4) GGA with TBE	1.89	1.33–2.68	0.0004
(5) Consolidation with TBE	1.06	0.97–1.17	0.2075
(6) Honeycombing	1.61	1.05–2.48	0.0280

GGA areas of ground-glass attenuation; *TBE* traction bronchiectasis or bronchiolectasis

[a] *HR* Hazard ratios are calculated with per 10%-increase unit

[b] *CI* confidence interval

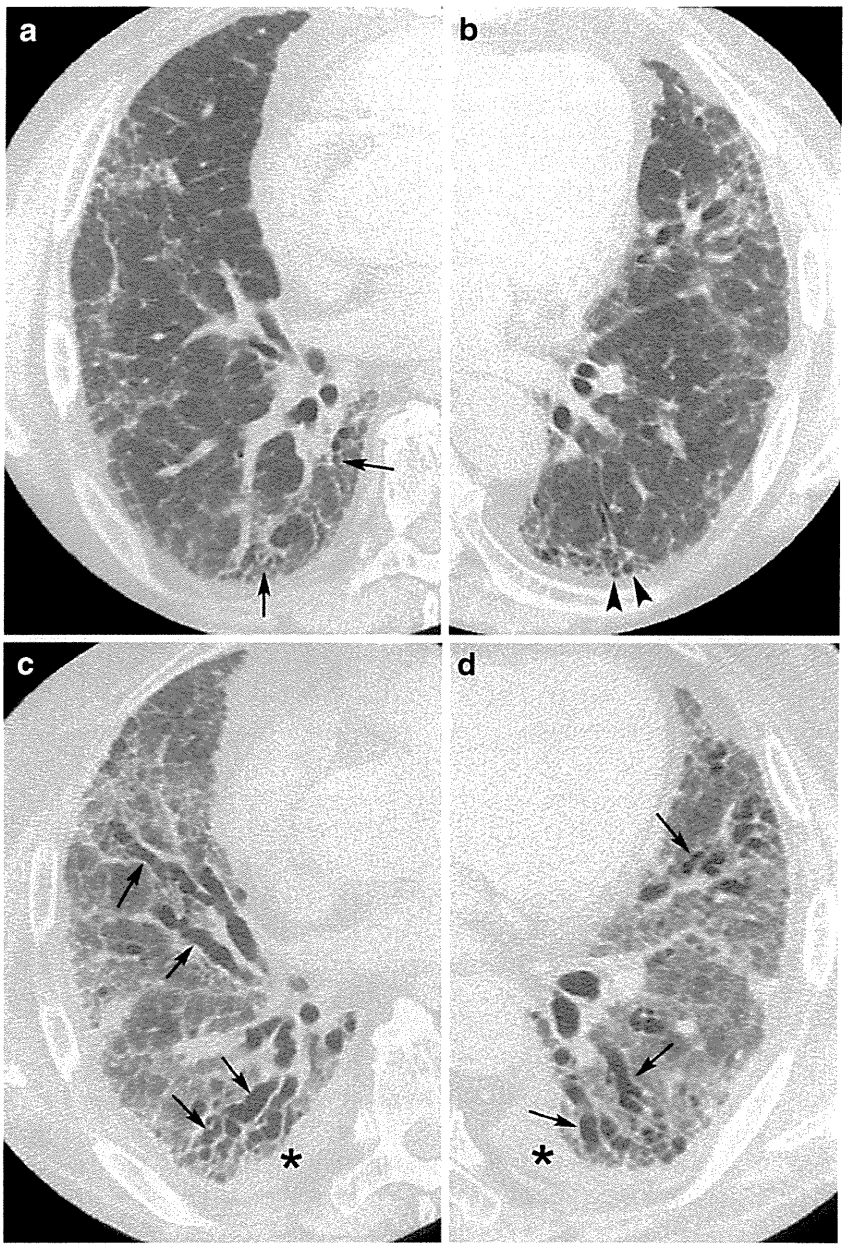

Fig. 2 A 71-year-old man with IPF and with acute exacerbation. **a, b** HRCT images at diagnosis of IPF show subpleural predominant interstitial fibrosis and small areas of GGA with traction bronchiolectasis (*arrows*) and honeycombing (*arrowheads*). **c, d** HRCT images at the onset of acute exacerbation (5 months after images **a** and **b**) show diffuse areas of GGA superimposed on underlying fibrotic opacities seen in images **(a)** and **(b)**. Marked traction bronchiectasis and bronchiolectasis (*arrows*) and architectural distortion are also seen. Note bilateral small pleural effusion (*asterisks*). The HRCT score showed 383 points. This patient died 10 days after the CT image

lying subpleural reticular opacities with honeycombing [5, 8, 9]. In the present study it was suggested that the extent score for areas of GGA with traction bronchiectasis or bronchiolectasis is one of the important findings related to prognosis.

Among the clinical and laboratory data in the present study, serum KL-6 values at the onset of AEx-IPF were significantly related to prognosis on univariate analysis. Sakamoto, et al. [26] reported that correlation between KL-6 levels and HRCT findings (GGA and traction bronchiectasis) were statistically significant in patients with fibrosing nonspecific interstitial pneumonia.

AEx-IPF histologically manifests as acute or organizing DAD, or, less commonly, OP [9, 11, 12]. On CT, OP presents as patchy areas of parenchymal opacification or nodular/mass-like opacities, with air bronchogram [27, 28]. Mild cylindrical bronchial dilatation is commonly evident in areas of parenchymal opacification, but traction bronchiectasis or bronchiolectasis with reticulation is rarely seen. Ichikado et al. [15, 16] compared CT findings with histopathologic findings of DAD and detected a close correlation between CT findings and pathologic phases of DAD. They determined that patients who had areas of GGA or airspace consolidation associated with traction bronchiectasis on CT had histological findings of the late proliferative or fibrotic phases of DAD, whereas patients who had GGA or consolidation without traction bronchiectasis had histologic features of the exudative or early proliferative phases of DAD [17]. Further, they reported that patients with CT

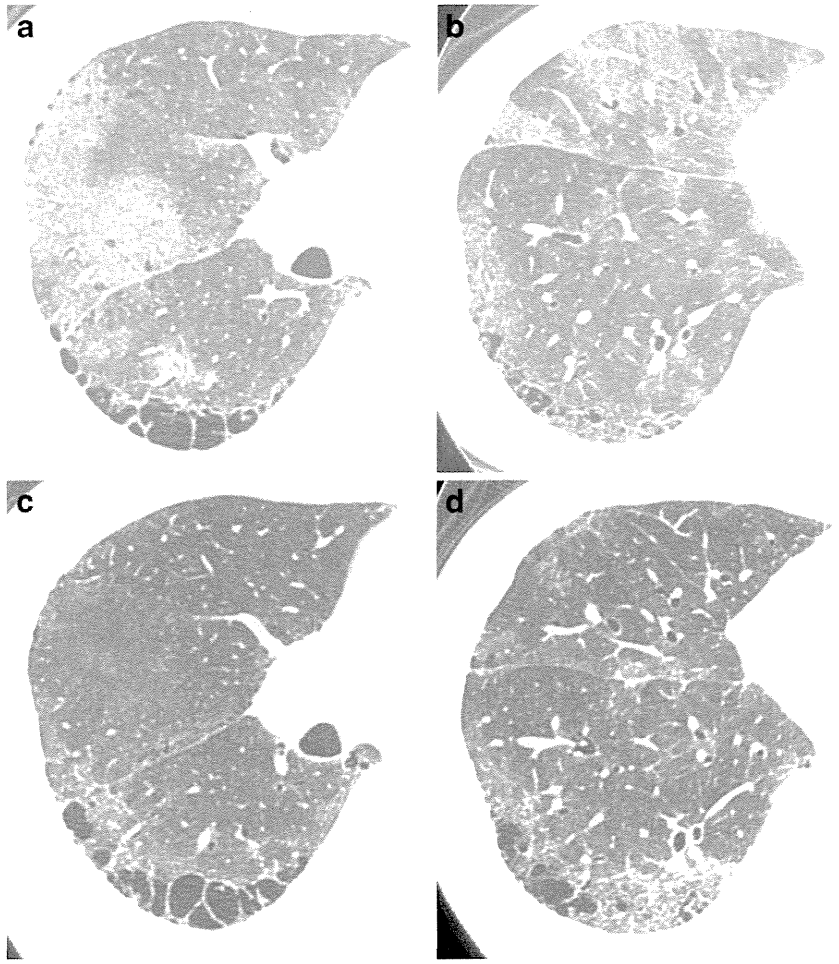

Fig. 3 A 70-year-old man with pathologically proven IPF/UIP and with acute onset of dyspnoea. HRCT images of the right lung at 4 cm below the tracheal carina (**a**) and 3 cm below the inferior pulmonary vein (**b**) at onset of acute exacerbation show extensive areas of GGA and increased attenuation superimposed on intralobular reticular opacities and subpleural air cysts including honeycombing (multifocal pattern of CT distribution). There were relatively small areas of ground-glass opacity with traction bronchiectasis or bronchiolectasis. The HRCT score showed 170 points at this time. HRCT images (**c** and **d**) at 28 days after onset of acute exacerbation (after corticosteroid and immunosuppressive therapy) show decrease in areas of GGA and improvement of lung attenuation. The patient recovered from mechanical ventilation and showed no evident deterioration at least after 12 months follow-up

findings suggestive of the late proliferative or fibrotic phases, including architectural distortion and areas of increased attenuation with associated bronchiectasis or bronchiolectasis, were less likely to survive than were patients without evidence of fibroproliferation [17]. Thus, traction bronchiectasis or bronchiolectasis within areas of increased parenchymal opacification on HRCT is a possible sign of progression from the exudative to the fibroproliferative and fibrotic stages of DAD.

In the present study the overall HRCT score at presence of AEx was the most important independent prognostic factor on multivariable analysis. This scoring system showed good interobserver agreement and the cutoff value of 245 revealed highly accurate performance (PPV and NPV, 0.96 and 0.77, respectively) for predicting patient's outcome. The HRCT score in the present study adapted from Ichikado et al. has been previously shown to be an independent prognostic factor for patients with ARDS secondary to pneumonia or sepsis [18] and in acute interstitial pneumonia (i.e., idiopathic ARDS) [17], other than AEx-IPF. Their results in addition to our results suggested that this HRCT scoring system is useful in determining the patient outcome for acute and progressive fibroproliferative pulmonary diseases.

Akira et al. [14] reported that prognosis in AEx was worse in patients with the new multifocal or diffuse parenchymal opacification as compared to peripheral

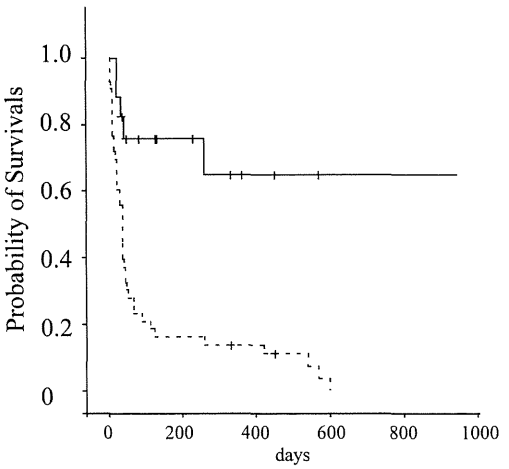

Fig. 4 Kaplan-Meier survival curves show the cause-specific survival according to the cut-off value of the HRCT score. Patients with a higher score (≥245) (n=48, *dotted line*) had a significant worse prognosis than did those with lower score (<245) (n=12, *solid line*) (log-lank test, P<0.0001)

opacification. Silva et al. [12] reported 24 cases with AEx superimposed on underlying chronic interstitial pneumonia including 12 cases with IPF/UIP. Their results showed no significant difference between survivors and non-survivors in the distribution CT patterns in all 24 cases even if assessing 12 IPF/UIP cases. Similar to the findings of Silva et al. [12], univariate analysis in the current study revealed that CT distribution did not show significant correlation with the patient outcome. In the present study the criteria for the AEx-IPF were different from those by Akira et al. [14] and disease severity and mortality of the patients in the present study were worse than their results. The difference of entry criteria may have caused the difference of disease background, for example, probability of DAD and OP patterns as an acute lung injury pattern.

There are a few limitations to our study. First, it was retrospective and did not allow correlation between the HRCT and the histopathologic findings. Because of its retrospective nature there was limited clinical and laboratory data available for review. Although a major effort was made to exclude patients with infection, the retrospective nature of the study and the limited availability of bronchoalveolar lavage, serology results, and histologic confirmation made it difficult to exclude infection in all cases. Second, the study involved a small number of patients. A prospective study with a substantially larger sample is needed to further validate our findings.

In summary, HRCT abnormalities indicative of fibroproliferative changes, in particular, extent areas of GGA with traction bronchiectasis or bronchiolectasis superimposed on underlying HRCT opacities consistent with UIP pattern are independently predictive of poor prognosis. In the present study, statistical significant difference in the survival rate was shown between the patients with lower CT score (<245) and with higher CT score (≥ 245).

We conclude that the HRCT score at AEx is independently related to prognosis in patients with AEx-IPF.

Acknowledgements This study was partially supported by a Grant to the Diffuse Lung Disease Group from the Ministry of Health, Labour and Welfare (Japan).

References

1. American Thoracic Society/European Respiratory Society (2002) American Thoracic Society/European Respiratory Society international multidisciplinary consensus classification of the idiopathic interstitial pneumonias. Am J Respir Crit Care Med 165:277–304
2. Martinez FJ, Safrin S, Weycker D et al (2005) The clinical course of patients with idiopathic pulmonary fibrosis. Ann Intern Med 142:963–967
3. Kondoh Y, Taniguchi H, Kawabata Y, Yokoi T, Suzuki K, Takagi K (1993) Acute exacerbation in idiopathic pulmonary fibrosis: analysis of clinical and pathologic findings in three cases. Chest 103:1808–1812
4. Akira M, Hamada H, Sakatani M, Kobayashi C, Nishioka M, Yamamoto S (1997) CT findings during phase of accelerated deterioration in patients with idiopathic pulmonary fibrosis. AJR Am J Roentgenol 168:79–83
5. Ambrosini V, Cancellieri A, Chilosi M et al (2003) Acute exacerbation of idiopathic pulmonary fibrosis: report of a series. Eur Respir J 22:821–826
6. Taniguchi H, Kondoh Y (2004) Revised criteria for acute exacerbation of idiopathic pulmonary fibrosis. The Annual Report by Study Group of Ministry of Health and Welfare for Diffuse Lung Disease, pp 114–119
7. Parambil JG, Myers JL, Ryu JH (2005) Histopathologic features and outcome of patients with acute exacerbation of idiopathic pulmonary fibrosis undergoing surgical lung biopsy. Chest 128:3310–3315
8. Kim DS, Park JH, Park BK, Lee JS, Nicholson AG, Colby T (2006) Acute exacerbation of idiopathic pulmonary fibrosis: frequency and clinical features. Eur Respir J 27:143–150
9. Collard HR, Moore BB, Flaherty KR et al (2007) Acute exacerbations of idiopathic pulmonary fibrosis. Am J Respir Crit Care Med 176:636–643
10. Taniguchi H, Ebina M, Kondoh Y et al (2010) Pirfenidone in idiopathic pulmonary fibrosis. Eur Respir J 35:821–829
11. Churg A, Müller NL, Silva CIS, Wright JL (2007) Acute exacerbation (acute lung injury of unknown cause) in UIP and other forms of fibrotic interstitial pneumonias. Am J Surg Pathol 31:277–284
12. Silva CIS, Müller NL, Fujimoto K et al (2007) Acute exacerbation of chronic interstitial pneumonia: high-resolution computed tomography and pathologic findings. J Thorac Imag 22:221–229
13. Song JW, Hong SB, Lim CM, Lim CM, Koh Y, Kim DS (2011) Acute exacerbation of idiopathic pulmonary fibrosis: incidence, risk factors, and outcome. Eur Respir J 37:356–363
14. Akira M, Kozuka T, Yamamoto S, Sakatani M (2008) Computed tomographic findings in acute exacerbation of idiopathic pulmonary fibrosis. Am J Respir Crit Care Med 178:372–378
15. Ichikado K, Johkoh T, Ikezoe J et al (1997) Acute interstitial pneumonia: high-resolution CT findings correlated with pathology. AJR Am J Roentgenol 168:333–338
16. Ichikado K, Suga M, Gushima Y et al (2000) Hyperoxia-induced diffuse alveolar damage in pigs: correlation between thin-section CT and histopathologic findings. Radiology 216:531–538
17. Ichikado K, Suga M, Müller NL et al (2002) Acute interstitial pneumonia: comparison of high-resolution computed tomography findings between survivors and non-survivors. Am J Respir Crit Care Med 165:1551–1556
18. Ichikado K, Suga M, Muranaka H et al (2006) Prediction of prognosis for acute respiratory distress syndrome with thin-section CT: validation in 44 cases. Radiology 238:321–329
19. World Medical Association (2008) Declaration of Helsinki: ethical principles for medical research involving human subjects, 2008 version (59th World Medical Association General Assembly, Seoul, October 2008). World Health Organization, Geneva, Available via http://www.wma.net/en/30publications/10policies/b3/index.html. Accessed 1 Jan, 2011
20. Hansell DM, Bankier AA, MacMahon H, McLoud TC, Müller NL, Remy J (2008) Fleischner Society: glossary terms for thoracic imaging. Radiology 246:697–722
21. Sumikawa H, Johkoh T, Colby TV et al (2008) Computed tomography findings in pathological usual interstitial pneumo-

nia: relationship to survival. Am J Respir Crit Care Med 177:433–439
22. Kundel HL, Polansky M (2003) Measurement of observer agreement. Radiology 228:303–308
23. Bland JM, Altman DG (1986) Statistical methods for assessing agreement between two methods of clinical measurement. Lancet 1(8476):307–310
24. Akobeng AK (2007) Understanding diagnostic tests 3: receiver operating characteristic curves. Acta Paediatr 96:644–647
25. Bernard GR, Artigas A, Brigham KL et al (1994) The American-European Consensus Conference on ARDS: definitions, mechanisms, relevant outcomes, and clinical trial coordination. Am J Respir Crit Care Med 149:818–824
26. Sakamoto K, Taniguchi H, Kondoh Y et al (2010) Serum KL-6 in fibrotic NSIP: correlations with physiologic and radiologic parameters. Respir Med 104:127–133
27. Lee KS, Kullnig P, Hartman TE, Müller NL (1994) Cryptogenic organizing pneumonia: CT findings in 43 patients. AJR Am J Roentgenol 162:543–546
28. Akira M, Yamamoto S, Sakatani M (1998) Bronchiolitis obliterans organizing pneumonia manifesting as multiple large nodules or masses. AJR Am J Roentgenol 170:291–295

OPEN ACCESS Freely available online

PLOS | ONE

The Role of Nucleus Accumbens Core/Shell in Sleep-Wake Regulation and their Involvement in Modafinil-Induced Arousal

Mei-Hong Qiu[1*☯], Wei Liu[2☯], Wei-Min Qu[2,3], Yoshihiro Urade[4], Jun Lu[2,5], Zhi-Li Huang[1,2,3*]

1 State Key Laboratory of Medical Neurobiology, Shanghai Medical College of Fudan University, Shanghai, China, **2** Department of Pharmacology, Shanghai Medical College of Fudan University, Shanghai, China, **3** Institutes of Brain Science, Fudan University, Shanghai, China, **4** Department of Molecular Behavioral Biology, Osaka Bioscience Institute, Suita, Osaka, Japan, **5** Department of Neurology, Beth Israel Deaconess Medical Center and Harvard Medical School, Boston, Massachusetts, United States of America

Abstract

Background: We have previously shown that modafinil promotes wakefulness via dopamine receptor D_1 and D_2 receptors; however, the locus where dopamine acts has not been identified. We proposed that the nucleus accumbens (NAc) that receives the ventral tegmental area dopamine inputs play an important role not only in reward and addiction but also in sleep-wake cycle and in mediating modafinil-induced arousal.

Methodology/Principal Findings: In the present study, we further explored the role of NAc in sleep-wake cycle and sleep homeostasis by ablating the NAc core and shell, respectively, and examined arousal response following modafinil administration. We found that discrete NAc core and shell lesions produced 26.5% and 17.4% increase in total wakefulness per day, respectively, with sleep fragmentation and a reduced sleep rebound after a 6-hr sleep deprivation compared to control. Finally, NAc core but not shell lesions eliminated arousal effects of modafinil.

Conclusions/Significance: These results indicate that the NAc regulates sleep-wake behavior and mediates arousal effects of the midbrain dopamine system and stimulant modafinil.

Citation: Qiu M-H, Liu W, Qu W-M, Urade Y, Lu J, et al. (2012) The Role of Nucleus Accumbens Core/Shell in Sleep-Wake Regulation and their Involvement in Modafinil-Induced Arousal. PLoS ONE 7(9): e45471. doi:10.1371/journal.pone.0045471

Editor: Giorgio F. Gilestro, Imperial College London, United Kingdom

Received May 22, 2012; **Accepted** August 22, 2012; **Published** September 19, 2012

Funding: This study was supported in part by grants-in-aid for scientific research from the National Natural Science Foundation of China (30970955, 30901797, 31171049, 31171010, 31121061), the Shanghai Committee of Science and Technology (11ZR1401800, 10441901600), National Basic Research Program of China grants (2009CB5220004, 2011CB711004), Shanghai Leading Academic Discipline Project (B119), China National Science and Technology Major Project for Drug Discovery (2009ZX09303-006) and Japan China Medical Association-Chinese Research support funding(2010). The funders had no role in study desigh, data collection and analysis, decision to publish, or preprartion of the manuscript.

Competing Interests: The authors have declared that no competing interests exist.

* E-mail: mhqiu@shmu.edu.cn (MHQ); huangzljp@yahoo.com.cn (ZLH)

☯ These authors contributed equally to this work.

Introduction

The nucleus accumbens (NAc) located in the ventral striatum is a part of the basal ganglia and limbic system. The NAc plays an important role in reward and addiction as well as aggression and fear [1–3]. Based on the neural make-up, projections and functions of the NAc [4–10], the NAc is divided into the core and shell.

Our previous lesion studies showed that NAc lesions by ibotenic acid caused a significant increase in the amount of wakefulness by an average of 27% across day-night. The wake increase was accompanied by sleep fragmentation (frequent sleep-wake transition and short sleep bout duration) [11]. These results reveal a novel role of the NAc in sleep-wake regulation. However, because the NAc lesions were mostly confined in the NAc core and in light of a recent study showing that NAc shell adenosine A_{2A} receptors mediated arousal effects of caffeine [12], it is crucial to investigate if the NAc shell is also involved in sleep-wake regulation.

Modafinil is one of most popular stimulants [13,14]. Dopamine transporter (DAT) knockout mice show elevated extracellular dopamine and a blunt arousal response following modafinil but not caffeine administration [15], indicating that dopamine system mediates arousal effects of modafinil. Our recent study further demonstrated that both dopamine D_1 and D_2 receptors were involved in regulation of modafinil-induced arousal [16]. However, the neuronal circuitry that mediates arousal of dopamine and modafinil has not been identified. We hypothesized that the NAc innervated by the ventral tegmental area (VTA) dopaminergic neurons mediates arousal induced by modafinil.

In the present study, we selectively lesioned NAc core and shell in rats, and examined their basal sleep-wake changes and sleep rebound after 6 hrs sleep deprivation (SD) and arousal response following modafinil administration. We found that both NAc core and shell lesions increased wakefulness but core lesions had a bigger arousal effect, and that both lesions reduced sleep rebound after 6-hr SD. NAc core lesions but not NAc shell lesions blocked arousal response to modafinil.

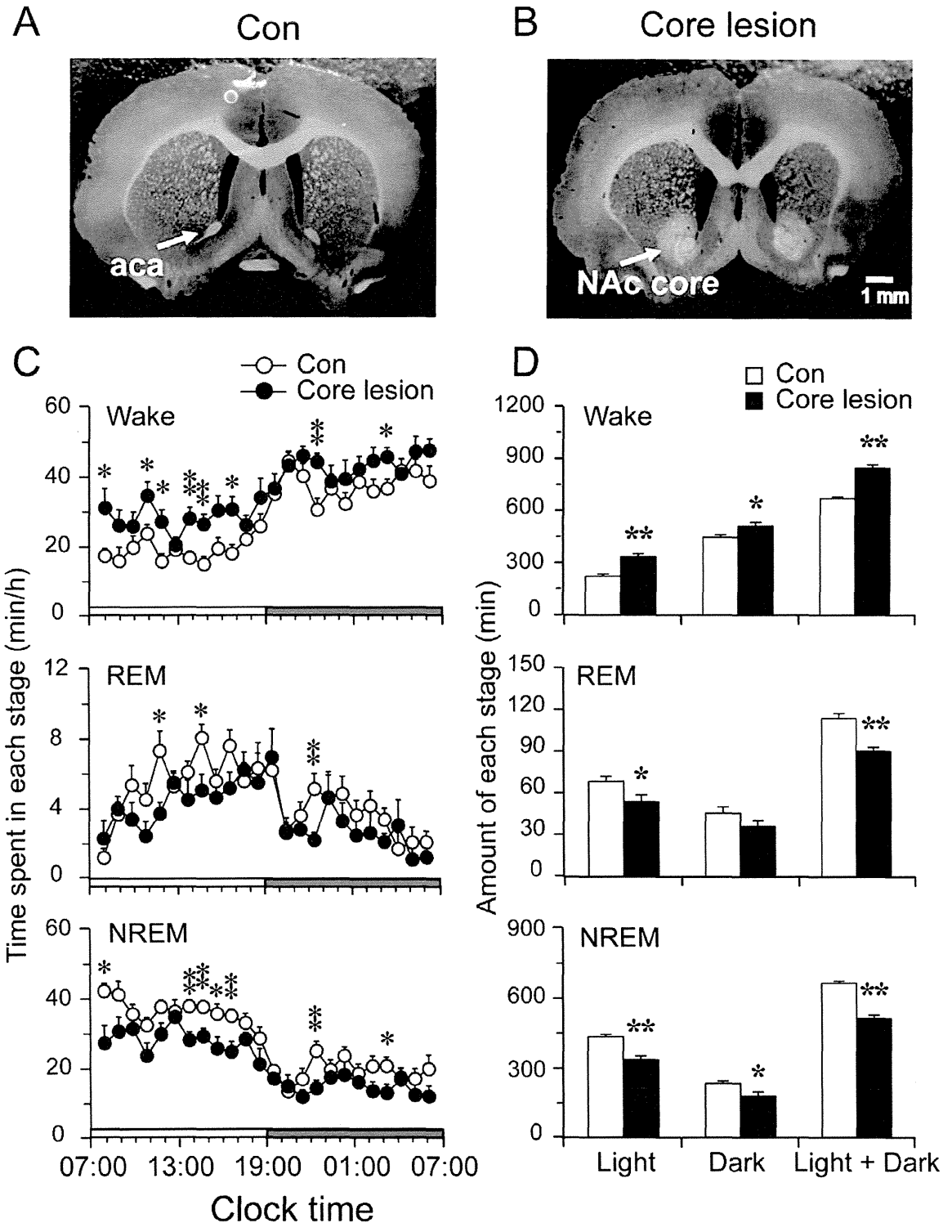

Figure 1. NAc core lesion increases wakefulness. A and B: photographs of representative coronal sections from a control (A) and a lesion case (B), the pale parts in B show the lesion in NAc core. Scale bar: 1 mm. aca: anterior commissure, anterior part. C: The hourly amount of wakefulness, REM and NREM sleep of control and NAc core lesioned group. Each circle represents the hourly mean ± SEM of each stage. D: Total time spent in wakefulness, REM and NREM sleep during the light and dark periods and over the 24-h day. *p<0.05, **p<0.01.
doi:10.1371/journal.pone.0045471.g001

Materials and Methods

Animals

Pathogen-free adult male Sprague Dawley rats (275–300 g) were obtained from the Laboratory Animal Center, Chinese Academy of Sciences (Shanghai, China). The animals were housed in individual cages at a constant temperature (22±0.5°C) with a relative humidity (60±2%) on an automatically controlled 12:12 light/dark cycle (light on at 7 A.M.), and had free access to food and water. The experimental protocols were approved by the Committee on the Ethics of Animal Experiments of the University of Fudan, Shanghai medical college (Permit Number: 20110307-049) and the Animal Research Committee of Osaka Bioscience Institute. Every effort was made to minimize the number of animals used and any pain and discomfort experienced by the subjects.

Neurotoxin Injection

Under chloral hydrate anesthesia (10% in saline, 360 mg/kg), a burr hole was made and a fine glass pipette (1 mm glass stock, tapering slowly to a 10–20 micron tip) containing 1% ibotenic acid (Sigma, St Louis, MO, USA) was lowered to the NAc core (AP = +1.2 mm, ML = ±1.8 mm, DV = −7.0 mm) and NAc shell (AP = +1.6 mm, ML = ±0.7 mm, DV = −7.0, −6.6, −6.2 mm), as per the atlas of Paxinos and Watson [17]. Then the toxin (0.4 µl per side) was injected with nitrogen gas pulses of 20–40 psi using an air compression system previously described [18]. Control animals were injected with saline into NAc core or shell. After two additional minutes, the pipette was slowly withdrawn and the animals were then implanted with electrodes for recording electroencephalogram (EEG) and electromyogram (EMG).

EEG/EMG Recording and Sleep Scoring

Rats were chronically implanted with EEG and EMG electrodes for polysomnographic recordings. The implant consisted of 2 stainless steel screws (1 mm diameter) inserted through the frontal (AP = +2 mm, ML = +3 mm) and parietal bones (AP = −4 mm, ML = +3 mm), and a stainless steel screw (1.5 mm diameter) inserted on the left frontal bone (AP = +3 mm, ML = −3 mm) as a reference electrode. Two wire electrodes served as EMG electrodes were placed into the neck muscles. All electrodes were attached to a connector and fixed to the skull with dental cement.

The recording of EEG and EMG were performed by means of a slip ring, designed so that behavioral movement of the animal would not be restricted. After a 7 d recovery period, the animals were housed individually in transparent barrels and habituated to the recording cable for 3 d before polygraphic recordings. EEG/EMG signals were amplified and filtered (EEG: 0.5–30 Hz, EMG: 20–200 Hz), then digitized at a sampling rate of 128 Hz, and recorded using SLEEPSIGN software [19]. When completed, polygraphic recordings were automatically scored off-line by 10 s epochs as wakefulness, REM, and NREM sleep by SLEEPSIGN according to standard criteria [20]. As a final step, defined sleep-wake stages were examined visually, and corrected, if necessary.

Sleep Deprivation

Rats were adapted in recording chambers for 3 days, and monitored for EEG and EMG for 2 consecutive days. The first day served as the baseline day; and on the second day the animals were subjected to a total sleep deprivation for 6 h (from 13:00 to 19:00) by lightly tapping via a soft tissue ball [21].

Pharmacological Treatments

Modafinil (Sigma-Aldrich) was dissolved in sterile saline containing 10% DMSO and 2% (w/v) cremophor immediately before use and administered intraperitoneally (i.p.) at 9 A.M. on the experimental day at a dose of 90 mg/kg. For baseline date, rats were injected i.p. with vehicle at 9 A.M.

Histochemistry

Animals were deeply anesthetized with 500 mg/kg of chloral hydrate and transcardially perfused with 50 ml saline, followed by 250 ml of neutral phosphate buffered 10% formalin. The brains were removed, cryoprotected in 20% sucrose at 4°C overnight and then sectioned at 30 µm on a freezing microtome in four series. One series of sections were processed for Nissl staining as described previously [11] to evaluate the extent of the lesions.

Statistical Analysis

The data were presented as the mean ± standard error of mean (SEM). The statistical significance of time course data for sleep–wake profiles, sleep amount, stage transition, the number of each stage bouts and mean duration were assessed by two-tailed unpaired t-test or one-way ANOVA followed by Dunnett's post hoc test. In all cases, $P<0.05$ was taken as the level of significance.

Results

Lesions of NAc Core and Shell cause a Robust Increase in Wakefulness

Consistent with our previous data [11], we observed that cell-specific lesions confined to NAc core (N = 10,typical examples of coronal sections photographs were shown in Fig. 1A and B) produced a robust 26.5% (838.9±89.7 versus 663.2±113.1 min in the control group, $p<0.01$) wake increase accompanied by a reduction in REM and NREM sleep per day (Fig. 1C and D), especially during the light period. NAc core lesions also disrupted sleep pattern, resulting more frequent sleep-wake state transition (Fig 2. A), or more wake and NREM sleep bouts and shorter duration of NREM sleep (Fig. 2B and C). The mean duration of NREM sleep was 28.5% (106.1±8.0 versus 148.5±4.5 sec, $p<0.01$) shorter than the control (Fig. 2C). Although the mean wake duration showed a tendency in lengthening, it did not reach statistical significance ($p>0.05$). We further calculated the distribution of NREM sleep and wake bouts and found that NAc core lesions particularly had more NREM sleep bouts in the ranges of 30–60 and 60–120 s but less in ranges of 240–480 and 480–960 s during the light period than control (Fig. 2D). The distribution of wake bouts did not show significant changes.

NAc shell lesion group (n = 9, typical photographs of histology of NAc shell lesions were shown in Fig. 3A) showed a 17.4% increase in wakefulness (820.6±9.2 versus 699.0±10.2 in the control group, $p<0.01$) (Fig. 3B and C), accompanied by a reduction in total NREM sleep. NAc shell lesions caused sleep fragmentation, more NREM sleep bouts with shorter average duration than control (Fig. 4). However, REM sleep change in term of duration and bout number did not reach statistical significance.

NAc Core and Shell Lesion Reduces Response of Sleep Homeostasis

To determine whether the NAc is involved in sleep homeostatic regulation, we performed a six hour SD from 13:00 to 19:00 in NAc core, NAc shell lesion group, and control group. The sleep time, EEG power spectra and the changes of characteristics of

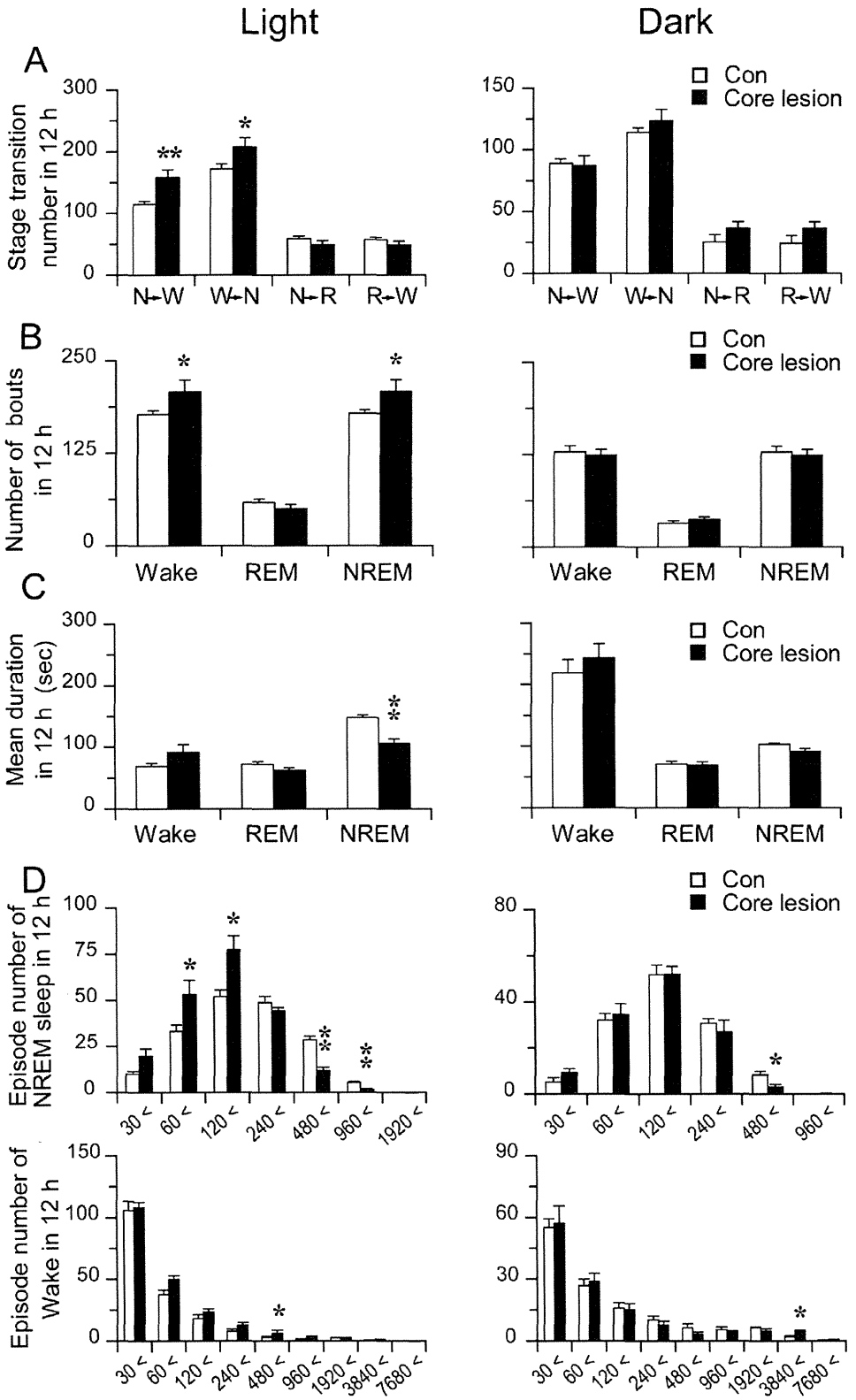

Figure 2. NAc core lesion causes sleep fragmentation. A: Sleep-wake stage transitions during the light and dark period (N, W and R represent NREM sleep, wakefulness and REM sleep, respectively). B and C: The number of bouts (B) and mean durations (C) during the light and dark periods. D: Distribution of number of NREM sleep and wake bouts across different episode durations during light and dark period. *$p<0.05$, **$p<0.01$.
doi:10.1371/journal.pone.0045471.g002

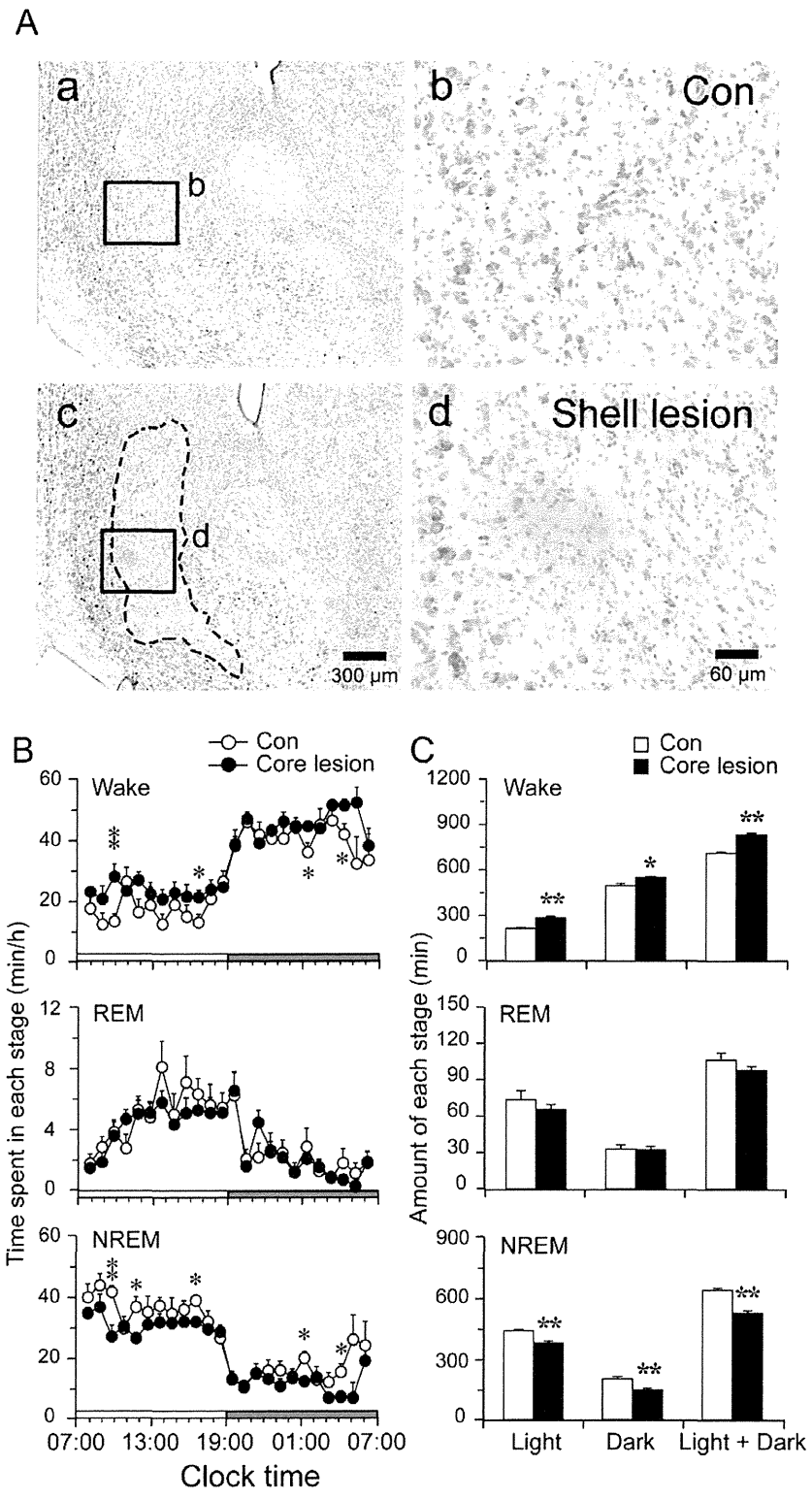

Figure 3. NAc shell lesion increases wakefulness. A: Representative thionin-stained coronal sections show intact control (a, b) and lesion (c, d) (b, d: high-magnification views of the rectangular areas marked in "a" and "c", respectively). Dotted lines in "c" outline the lesion area that matches the NAc shell. Scale bars are 300 μm in "a" and "c"; 60 μm in "b" and "d". B: The hourly amount of wakefulness, REM and NREM sleep of control and NAc shell lesioned rats. Each circle represents the hourly mean ± SEM of each stage. C: Total time spent in wakefulness, REM and NREM sleep during the light and dark period and 24-hours. *p<0.05, **p<0.01.
doi:10.1371/journal.pone.0045471.g003

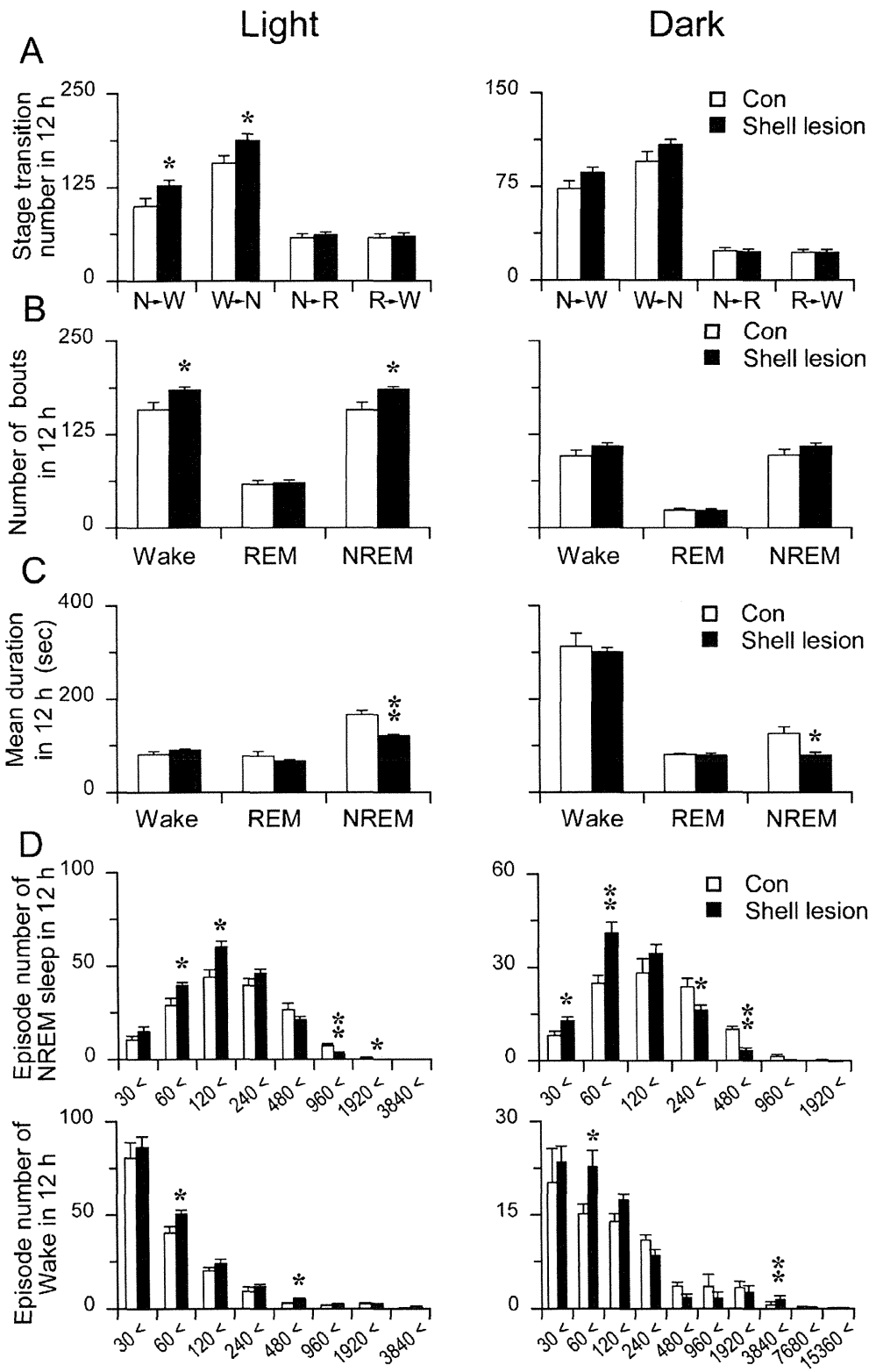

Figure 4. NAc shell lesion causes sleep fragmentation. A: Sleep-wake stage transitions during the light and dark period (N, W and R represent NREM, wakefulness and REM sleep, respectively). B and C: The number of bouts (B) and mean durations (C) during the light and dark periods. D: Number of NREM sleep and Wake bouts at different ranges of episode duration during the light and dark periods.*$p<0.05$, **$p<0.01$.
doi:10.1371/journal.pone.0045471.g004

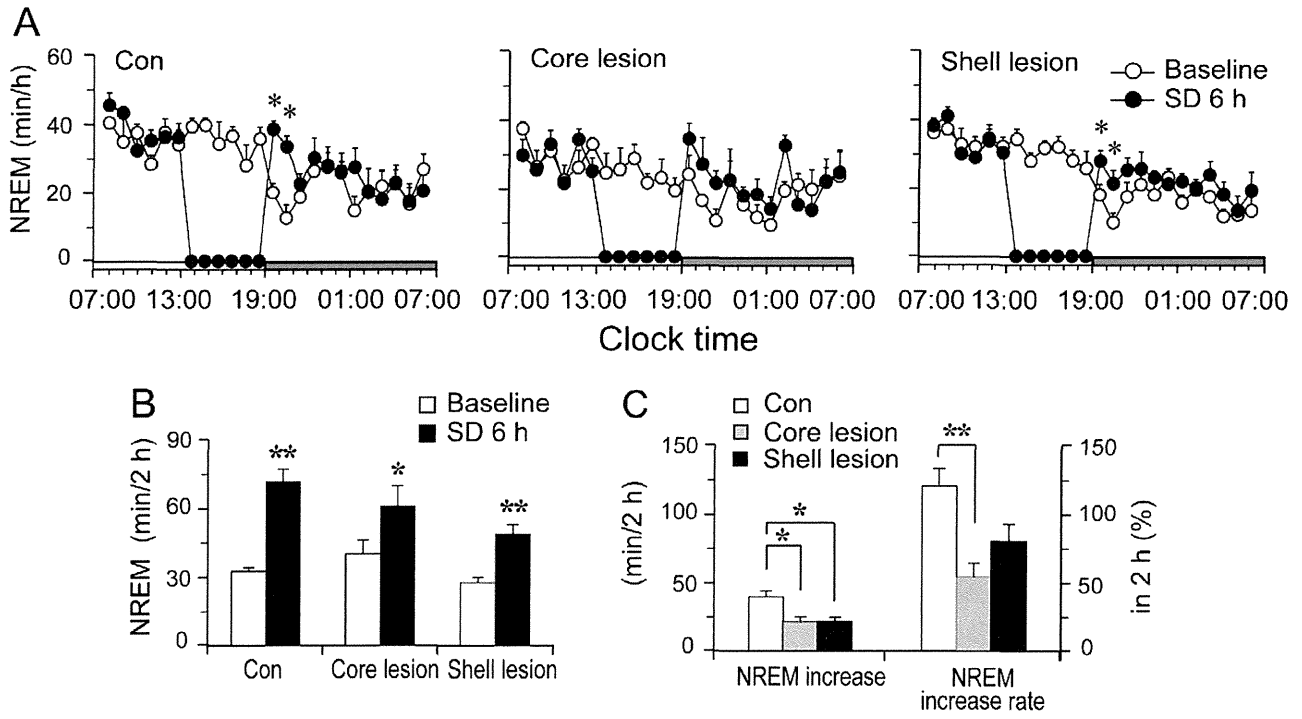

Figure 5. NAc lesions reduce sleep rebound. A: Time-course of NREM sleep in baseline and SD of control, NAc core and shell lesioned rats. SD was between 13:00 and 19:00. Each circle represents the hourly mean ± SEM of NREM sleep. B: Total time spent in NREM sleep in 2 h after SD. C: The absolute increased NREM sleep amounts and the percentage of NREM sleep increase in 2 h after SD of each group. *p<0.05, **p<0.01.
doi:10.1371/journal.pone.0045471.g005

sleep-wake episodes during NREM sleep in 6 hrs after SD over the baseline of the same period of prior day were used to determine and quantify the sleep rebound. Fig. 5A and B summarized the time-courses of the hourly amounts of NREM sleep, and the cumulative amounts of NREM sleep for two hours after SD. Control rats, following the SD, showed a marked increase in NREM sleep in first two hours (Fig. 5A, left panel). NAc core lesion group showed significant NREM sleep rebound in the first two hours ($p<0.05$, Fig. 5B), but this NREM sleep increase was significantly lower than the control (Fig. 5A, middle panel). Similarly, the NAc shell lesion group showed a significant sleep rebound, but the increase was significantly less than the control ($p<0.05$, Fig. 5C, left panel). The percentage increase of sleep rebound in the first two hours was 119.9±0.12% ($p<0.01$) in control group, 53.7±0.37% ($P<0.05$) in NAc core lesion group, and 79.6±0.14% ($p<0.01$) in NAc shell lesion group (Fig. 5B and C). Of these changes, NAc core lesion group showed the least rebound (Fig. 5C, right panel). REM sleep did not increase during the first hour after SD in control rats.

We further analyzed the EEG power spectra during NREM sleep in 6 hrs after SD among control, core lesion and shell lesion rats, The power of each 0.5 Hz bin was first averaged across the sleep stages individually and then normalized as a group by calculating the percentage of each bin from the total power (0–24.5 Hz) of the individual animal. As shown in Fig. 6A, following SD, EEG power density significantly increased in the frequency range of 1–2.5 Hz in control rats, and in the frequency range of 1–2 Hz in shell lesioned rats, whereas core lesioned rats did not show a significant change.

During the 6 hrs after SD, compared with their own baseline EEG, the bouts of each stage were not changed (Fig. 6B), while in control rats, the mean duration of wake episodes was decreased 25.3% ±9.1% ($p<0.05$), meanwhile the mean duration of NREM sleep episode was significantly increased by 51.1% ±13.3% ($p<0.01$). The NAc shell lesion group showed similar but less changes than the control ones. NAc core lesion group did not show changes in mean duration of wake and NREM sleep episodes (Fig. 6C).

To better understand sleep-wake profile following SD, we calculated distribution of NREM sleep bout duration (Fig. 6D). Control group showed less in the number of bout duration range of 30–60 and 60–120 sec but more in the range of 120–240 and 240–480 sec during the 6-hr sleep recovery period than that of the baseline. NAc shell lesioned group showed similar changes as control group, while core lesion group showed reduced effects.

NAc Core Lesion Blocks Modafinil-induced Arousal

In order to determine whether the NAc core or shell mediates arousal effects of modafinil, we injected vehicle or modafinil (90 mg/kg) at 9:00 A.M. in three groups of rats. Fig. 7A–F shows examples of polygraphic recordings and corresponding hypnograms for a rat of each group treated with vehicle or modafinil. To our surprise, vehicle injection in NAc core lesioned animals significantly induced more wakefulness than the control rats (83.7±8.2 versus 51.4±2.5 min in the control group, $p<0.05$, Fig. 8C). Modafinil induced continuous wakefulness for about 2 hrs in control and NAc shell lesioned rats (Fig. 7B and F; Fig. 8A, E and F), which was significantly longer than vehicle injection. In the NAc core lesioned rats, modafinil produced about 1.5 hrs continuous wakefulness, and which was not significantly different from its vehicle injection (Fig. 7C and D; Fig. 8B and C). Next, we investigated the sleep latency in rats injected with modafinil. Sleep latency was defined as the time from the injection of modafinil or vehicle to the appearance of the first NREM sleep episode lasting

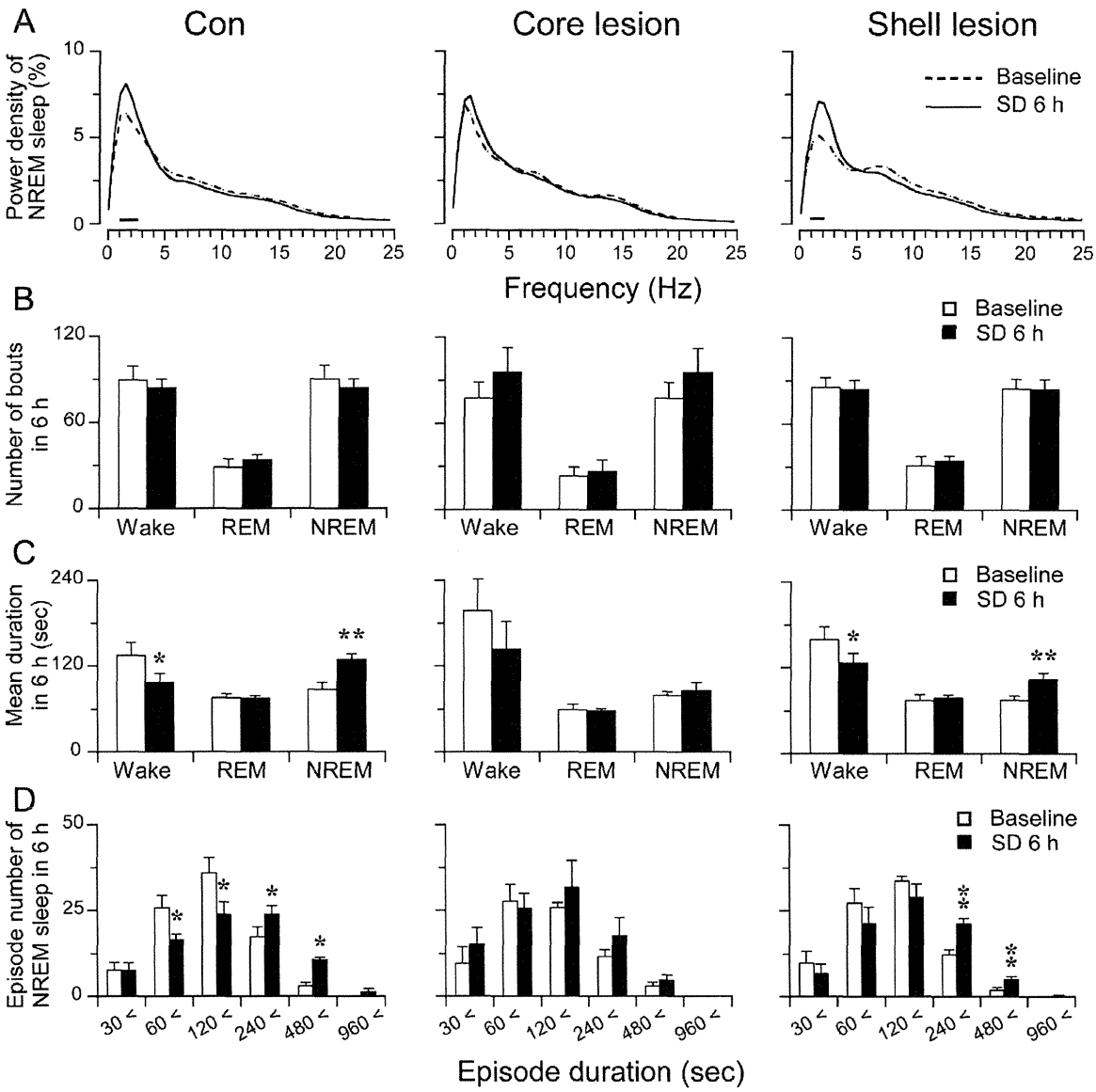

Figure 6. Power spectrum and stage analysis of sleep homeostatic response. A: Relative average EEG power density of NREM sleep during the first 6 hrs after SD. The horizontal bars indicate statistical difference ($p<0.05$) between SD and baseline of each group. B: Total number of wake, REM and NREM sleep bouts in the first 6 hrs after SD. C:Mean duration of wake, REM and NREM sleep in the first 6 hrs after SD. D: Changes in number of NREM sleep bouts at different ranges of episode duration in the first 6 hrs after SD. *$p<0.05$, **$p<0.01$.
doi:10.1371/journal.pone.0045471.g006

for at least 20 s [22]. As shown in Fig. 7G and H, modafinil significantly prolonged the NREM sleep latency in control group. In core lesioned group, sleep latency of modafinil was significantly decreased. Interestingly, vehicle injection also produced similar sleep latency as the modafinil injection (Fig. 7G) in core lesioned group. Shell lesion did not affect the effect of modafinil on sleep latency (Fig. 7H).

The net wake increase in two hours after modafinil injection vs vehicle injection were 59±4.0 min in control group (Fig. 8C and D). The percentage increase of wakefulness after modafinil over vehicle injection was 116.8±12.1% in control group and 12.3±10.9% in NAc core lesioned group (Fig. 8C and D).

Rats with NAc shell lesions showed similar arousal response and NREM sleep latency to modafinil as the control rats (Fig. 8E–H).

Discussion

In the present study, we demonstrated that lesions of both NAc core and shell produced a significant wake increase, and reduced sleep homeostatic response, with NAc core lesions showing a strong effect. NAc core lesions but not NAc shell lesions blocked arousal response to modafinil.

Our previous observation [11] showed that bilateral striatal lesions resulted in a significant reduction in time spent in wakefulness, as well as fragmentation of both sleep and wakefulness. However, when the striatal lesions include the NAc, their effect on wakefulness is attenuated. Consistent with this observation, lesions restricted to the whole NAc produce an increase in wakefulness and a reduced duration of bouts of NREM sleep. These findings suggest that the dorsal and ventral striatum play

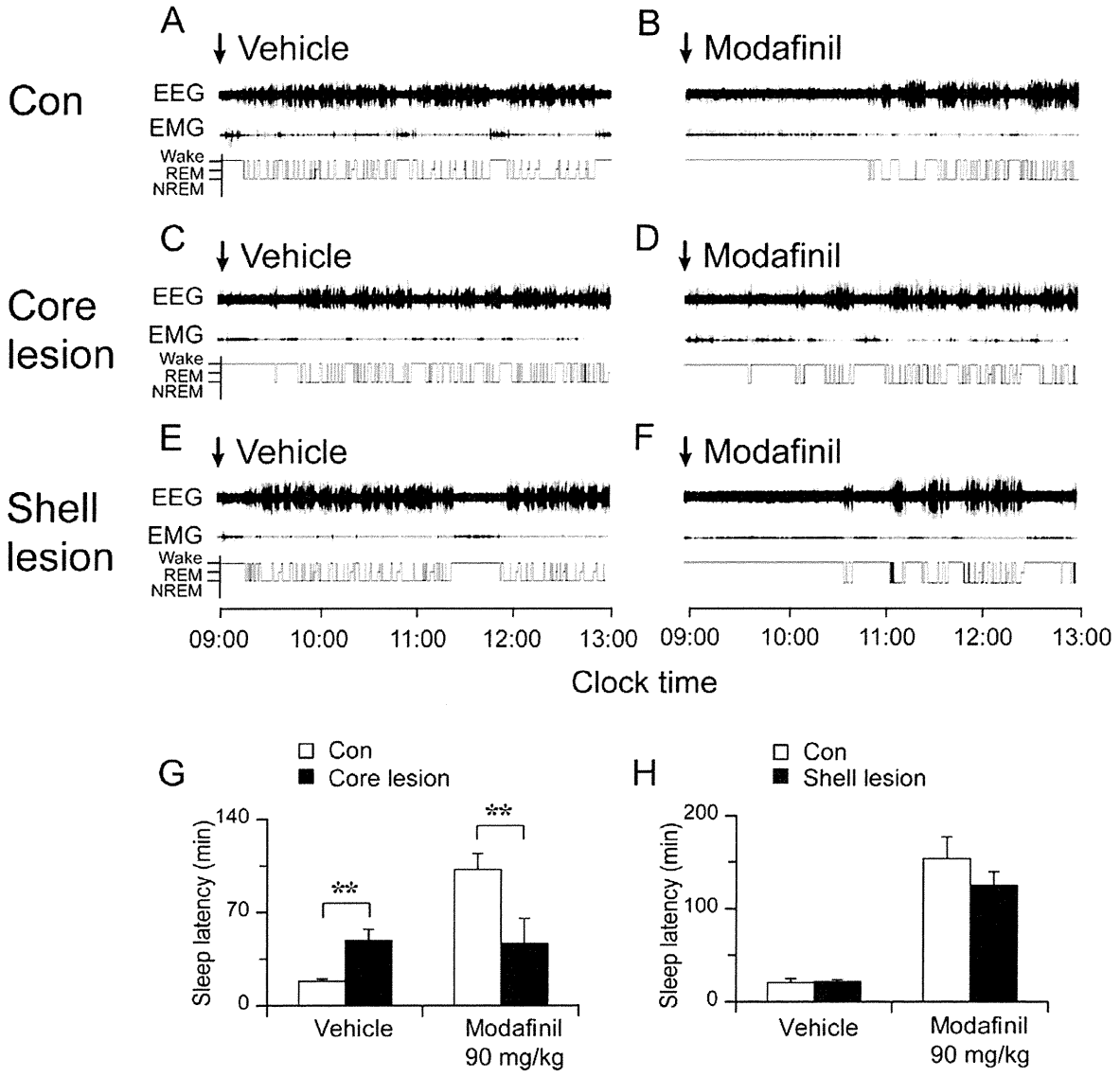

Figure 7. NAc core lesion reduces sleep latency following modafinil administration. Examples of polygraphic recordings and corresponding hypnograms in control, NAc core and shell lesioned rats treated with vehicle (A, C and E) and modafinil at the dose of 90 mg/kg (B, D and F). The arrows indicate the time of vehicle or modafinil injection. G and H: Effect of modafinil on NREM sleep latency in NAc core lesioned, shell lesioned and their control rats. *p<0.05, **p<0.01.
doi:10.1371/journal.pone.0045471.g007

opposing roles in sleep–wake regulation: the caudate–putamen (or dorsal striatum) enhances wakefulness whereas the NAc (or ventral striatum) promotes sleep. The present study aimed to elucidate the role of core or shell in sleep-wake regulation. We used a low concentration of ibotenic acid (1.0%, 400 nl per side) to make the core lesion more restricted, whereas the former study used a high concentration (10%, 45 nl per side) of ibotenic acid which made core lesion to partially damage the shell. In general, NAc core and shell lesion rats exhibited a similar phenotype in increased wakefulness, and sleep fragmentation (more sleep-wake transitions, reduced NREM sleep mean duration, and increased episode numbers for wake and sleep). These changes mainly occurred during the light period, indicated that NAc core and shell lesions resulted in the instability of NREM sleep under baseline conditions, especially in their inactive period.

After a 6-hr SD, the control rats showed a significant sleep rebound as indicated by an increase of NREM sleep amount with enhanced delta EEG power and increased mean duration and the number of long bouts during the first 6 hr period post SD, However NAc core lesioned rats did not show the prolongation of NREM sleep and enhancement of sleep intensity and consolidation. NAc shell lesion group showed similar but less prominant changes, compared with the control ones. The reduced sleep rebound after SD in NAc core and shell lesion suggests that NAc is involved in sleep homeostatic regulation.

Unlike psychostimulants such as methamphetamine, modafinil does not have strong psychological dependence and abused tendency [23–26]. On the other hand, like pyschostimulants, modafinil's arousal property depends on the dopamine system [27,28]. Mice with DAT knockout that have high extraceullar

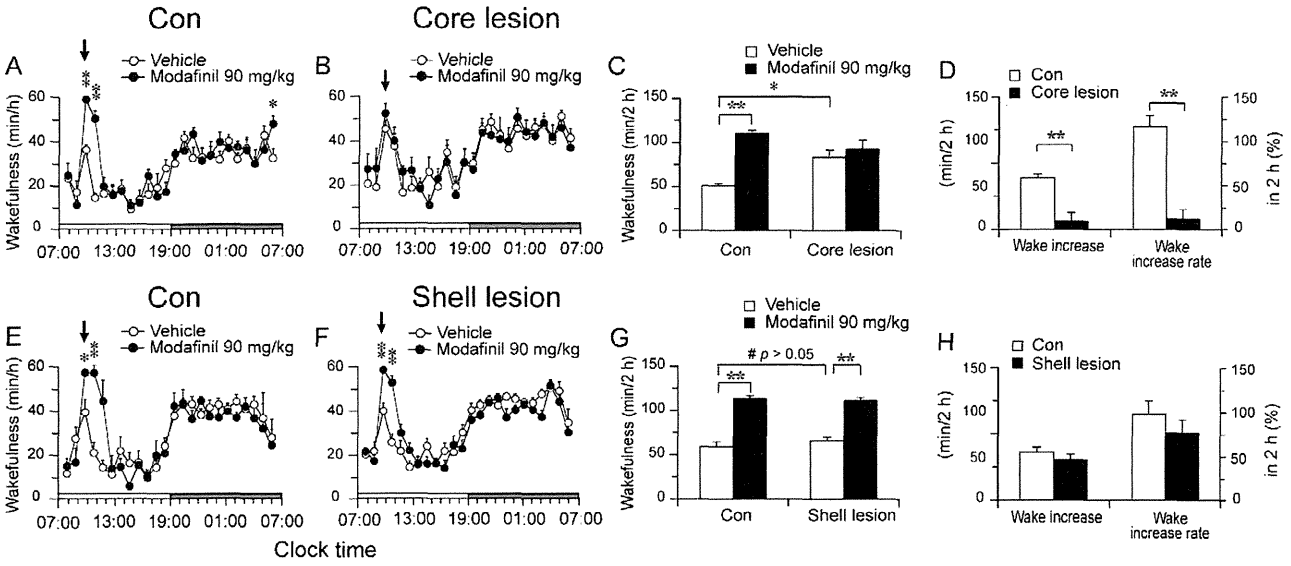

Figure 8. NAc core lesion blocks modafinil-induced arousal. A, B, E and F: Time course changes of wakefulness produced by i.p. administration of vehicle or modafinil (90 mg/kg). Each circle represents the hourly mean ± SEM. Arrows indicate the injection time (9 A.M.). C and G: Total time spent in wakefulness during two hours after the vehicle and modafinil administration. D and H: The increased wakefulness (min) and the percentage of wake increase in two hours after modafinil administration of each group. *p<0.05, **p<0.01.
doi:10.1371/journal.pone.0045471.g008

dopamine do not produce a wake response following modafinil administration [15], and dopamine D_2 receptor knockout mice treated with a D_1 receptor antagonist abolish the arousal effects by modafinil [16]. Although orexin and histamine systems are activated by modafinil [29,30], they may not be essential for the arousal effects of modafinil as orexin and histidine decarboxylase (an enzyme for histamine synthesis) knockout mice have a normal arousal response to modafinil [15,31,32]. Core lesion but not shell lesion abolished the arousal effects of madafinil, suggesting that dopamine receptors expressed in the core are essential for the arousal effects of modafinil.

The NAc core mediates arousal effects of modafinil. Interestingly, adenosine A_{2A} receptors in the NAc shell but not in NAc core play a pivotal role in regulation of caffeine-induced arousal [12]. It has been established that caffeine induces arousal via adenosine system, but not dopamine system [12,15,33,34]. Thus the NAc may be the hub that mediates multiple neurotransmitters including adenosine and dopamine for sleep-wake control [12,35,36].

How the NAc regulates sleep is not completely clear. The NAc has GABAergic projections to a wide range of targets, including the ventral pallidum, the lateral hypothalamus, the parabrachial nucleus and the VTA, that may contribute to wakefulness [37]. Therefore, it can be hypothesized that NAc activation exerts inhibitory effects on important arousal systems and promotes sleep. Although both core and shell are important in sleep-wake regulation, the mechanisms on different roles of these two parts in homeostasis regulation and in the arousal effects of modafinil/caffeine remain to be elucidated.

Author Contributions

Conceived and designed the experiments: MHQ ZLH. Performed the experiments: MHQ WL. Analyzed the data: MHQ WL. Contributed reagents/materials/analysis tools: MHQ ZLH YU WMQ. Wrote the paper: MHQ JL ZLH.

References

1. Ross S, Peselow E (2009) The neurobiology of addictive disorders. Clin Neuropharmacol 32: 269–276.
2. Dalley JW, Fryer TD, Brichard L, Robinson ES, Theobald DE, et al. (2007) Nucleus accumbens D2/3 receptors predict trait impulsivity and cocaine reinforcement. Science 315: 1267–1270.
3. Zubieta JK, Stohler CS (2009) Neurobiological mechanisms of placebo responses. Ann N Y Acad Sci 1156: 198–210.
4. Chang JY, Sawyer SF, Lee RS, Woodward DJ (1994) Electrophysiological and pharmacological evidence for the role of the nucleus accumbens in cocaine self-administration in freely moving rats. J Neurosci 14: 1224–1244.
5. Jongen-Relo AL, Voorn P, Groenewegen HJ (1994) Immunohistochemical characterization of the shell and core territories of the nucleus accumbens in the rat. Eur J Neurosci 6: 1255–1264.
6. Betancur C, Rostene W, Berod A (1997) Chronic cocaine increases neurotensin gene expression in the shell of the nucleus accumbens and in discrete regions of the striatum. Brain Res Mol Brain Res 44: 334–340.
7. Stratford TR, Kelley AE (1997) GABA in the nucleus accumbens shell participates in the central regulation of feeding behavior. J Neurosci 17: 4434–4440.
8. Parkinson JA, Olmstead MC, Burns LH, Robbins TW, Everitt BJ (1999) Dissociation in effects of lesions of the nucleus accumbens core and shell on appetitive pavlovian approach behavior and the potentiation of conditioned reinforcement and locomotor activity by D-amphetamine. J Neurosci 19: 2401–2411.
9. Di Chiara G (2002) Nucleus accumbens shell and core dopamine: differential role in behavior and addiction. Behav Brain Res 137: 75–114.
10. Pothuizen HH, Jongen-Relo AL, Feldon J, Yee BK (2005) Double dissociation of the effects of selective nucleus accumbens core and shell lesions on impulsive-choice behaviour and salience learning in rats. Eur J Neurosci 22: 2605–2616.
11. Qiu MH, Vetrivelan R, Fuller PM, Lu J (2010) Basal ganglia control of sleep-wake behavior and cortical activation. Eur J Neurosci 31: 499–507.
12. Lazarus M, Shen HY, Cherasse Y, Qu WM, Huang ZL, et al. (2011) Arousal effect of caffeine depends on adenosine A2A receptors in the shell of the nucleus accumbens. J Neurosci 31: 10067–10075.
13. Zeitzer JM, Nishino S, Mignot E (2006) The neurobiology of hypocretins (orexins), narcolepsy and related therapeutic interventions. Trends Pharmacol Sci 27: 368–374.
14. Minzenberg MJ, Carter CS (2008) Modafinil: a review of neurochemical actions and effects on cognition. Neuropsychopharmacology 33: 1477–1502.